Journal of Sound and Vibration (2000) **233**(2), 311–327
doi:10.1006/jsvi.1999.2801, available online at http://www.idealibrary.com on IDEAL®

TIME DOMAIN BUFFETING ANALYSIS OF SUSPENSION BRIDGES SUBJECTED TO TURBULENT WIND WITH EFFECTIVE ATTACK ANGLE

Q. Ding, P. K. K. Lee and S. H. Lo

Department of Civil Engineering, The University of Hong Kong, Pokfulam Road, Hong Kong, People's Republic of China

(*Received* 9 *July* 1999, *and in final form* 24 *November* 1999)

Suspension bridges are long-span flexible structures susceptible to various types of wind-induced vibrations such as buffeting actions. In this paper, a three-dimensional finite element model formulated to deal with suspension bridges under turbulent wind with effective attack angle is presented. In this model, all sources of geometric non-linearity such as cable sag, force-bending moment interaction in the bridge deck and towers as well as changes in bridge geometry due to large displacements are fully considered. The wind loads which include buffeting loads and self-excited loads are converted into the time domain by using a computer simulation technique to form aerodynamic damping and stiffness matrices as well as element loading vectors. Furthermore, a more refined model of wind loads is constructed in order to investigate the effect of an instantaneous change in effective attack angle of turbulent wind on bridge buffeting response. By comparing the results with those obtained by classic buffeting theory through an example bridge, the validity of the presented method is verified.

1. INTRODUCTION

Early this century, with the rapid development of construction material and technology, many long-span suspension bridges were built all over the world. However, these bridges exhibit special characteristics such as high flexibility, low structural damping and light in weight, which are very susceptible to wind actions. The Tacoma disaster in 1940 has focused engineers' attentions on the vibration characteristics of suspension bridges and the responses to wind excitations. Since then, numerous researchers [1–7] have made significant contributions on the stability of suspension bridges under wind actions which form the foundation of bridge aeroelasticity.

Buffeting action is a type of vibration motion induced by turbulent wind. As natural wind is not steady but turbulent in character, wind fluctuations in the vertical and horizontal directions are random in space, and thus the wind pressures along the bridges are random in time and space. Depending on the spectral distribution of the pressure vectors, certain modes of vibration on the whole bridge may selectively be excited. In fact, these wind-induced buffeting actions are related not only to wind speed but also to the shape of the cross-section of the bridge deck and the interaction between the bridge and wind motion [8]. Unlike other wind-induced vibrations such as flutter, vortex shedding and galloping, the buffeting response does not generally lead to catastrophic failure. This is probably the reason that less attention has been paid to this aspect in the last two decades. However, with the record-breaking span lengths of modern suspension bridges, buffeting response is

0022-460X/00/220311 + 17 $35.00/0

greatly increased which may cause serious fatigue damages to structural components and connections, instability of vehicles travelling on the bridge deck and discomfort to pedestrians. By now, with the high expectation of the performance of modern suspension bridges, buffeting analysis is one of the most important aspects of structural reliability under turbulent wind.

The classic buffeting analysis method is mainly based on Scanlan's theory [5] in which flutter derivatives, joint acceptances as well as admittance functions are introduced to consider the temporal and spatial distributions of wind loads. However, this method resorts to model superposition, and hence ignores the coupling between the modes of vibration. On the other hand, due to limitations in the frequency domain, it cannot reflect the entire response procedure of bridge motions, and hence cannot supply enough information for the analysis of element fatigue and assessment of service comfortability of bridges under wind actions.

In this paper, a time domain buffeting analysis method is proposed to analyze the buffeting response of suspension bridges under turbulent wind in order to provide useful information for further study on element fatigue, bridge comfortability as well as bridge safety. In this method, a three-dimensional finite element model which takes into account all geometric non-linearity has been developed to model suspension bridges. Based on Scanlan's method, wind loads including buffeting loads and self-excited loads are described as functions of aerodynamic parameters which can be obtained through wind tunnel tests. These wind loads are converted into the time domain by using a computer simulation technique. In order to investigate the effect of the instantaneous change in effective attack angle of turbulent wind on bridge buffeting response, a more refined model of wind loads has been developed. Finally, the Newmark-β step-by-step numerical integration algorithm is used to calculate the buffeting responses of the bridge. By comparing the results with those obtained by classic buffeting theory, the validity of the proposed method has been confirmed.

2. WIND FORCES

According to the classical airfoil theory, it is assumed that the wind velocity at any one point along a bridge is composed of three components: one for the mean part U, one for the fluctuating part $u(x, t)$ in the along-wind direction and one for the fluctuating part $w(x, t)$ in the vertical direction. These three parts of wind components impose drag D, lift L and moment M on a bridge deck, as shown in Figure 1.

Normally, the total wind load is made up of the steady state wind loads, the buffeting loads and the self-excited loads. However, the steady state wind loads are only related to the mean part of the oncoming wind flow and are assumed to act on the bridge deck at all times during the buffeting consideration of the bridge. Therefore, these can be regarded as the static loads which only shift the bridge's equilibrium position to a new position and are not directly relevant to buffeting responses. In the following buffeting analysis, the effects of steady state wind loads are not taken into consideration.

2.1. BUFFETING LOADS

Buffeting loads are caused by the fluctuating part of the wind velocity of which the along-wind part u and the vertical part w are much smaller than the mean wind velocity U. By neglecting u^2, w^2 and uw, buffeting loads per unit span can be expressed according to

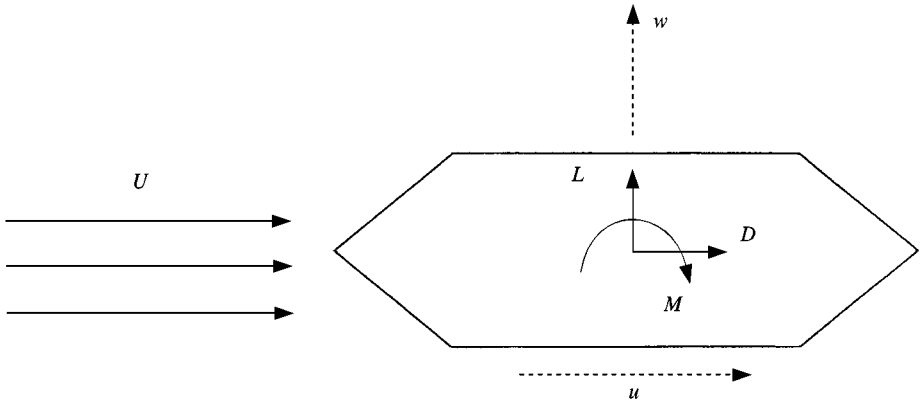

Figure. 1. Wind components at a point along bridge axis.

quasi-steady theory as follows:

$$L_b(x,t) = -\frac{1}{2}\rho U^2 B\left\{2C_L(\alpha_0)\frac{u(x,t)}{U} + \left[C'_L(\alpha_0) + \frac{A}{B}C_D(\alpha_0)\right]\frac{w(x,t)}{U}\right\}, \tag{1a}$$

$$M_b(x,t) = \frac{1}{2}\rho U^2 B^2\left[2C_M(\alpha)\frac{u(x,t)}{U} + C'_M(\alpha_0) + \frac{w(x,t)}{U}\right], \tag{1b}$$

$$D_b(x,t) = \frac{1}{2}\rho U^2 B\left[2\frac{A}{B}C_D(\alpha_0)\frac{u(x,t)}{U}\right], \tag{1c}$$

where ρ is the air density, C_D, C_L and C_M are the drag, lift and moment coefficients obtained by wind tunnel tests on cross-section model of the bridge, C'_L and C'_M are slopes of C_L and C_M, α_0 is the effective attack angle of the oncoming wind, A is the cross-wind projected area (per unit span) normal to the mean wind speed and B is the deck width.

Computer simulation technique is used to generate the fluctuating wind according to the wind spectrum recorded from the bridge site because it is quite difficult to obtain the representative fluctuating parts of wind in practice. Kovacs *et al.* [9] have presented a method to simulate the fluctuating wind velocity along a bridge deck. In their method, the fluctuating wind velocities $u(x,t)$ and $w(x,t)$ are assumed to consist of a series of components in the frequency domain from 0·001 to 1·5 Hz. This is the scale of the wind speed which has the greatest effect on the buffeting responses of bridges. Each component is a complex vector, i.e., each has an absolute size and a starting phase. The simulation takes place similar to a usual random signal in which the component vectors are rotated with the speed of their own angular velocity and are summed vectorially. The fluctuating wind velocity constitutes the real part of the resultant. The turbulent part of the momentary wind velocity in point x can be generated from Davenport's coherence formula [9] as in the following:

$$u(x,t) = \sum_j \left[\sqrt{\frac{2S(n_j)\Delta n}{\sum_k C^2(\xi_k, n_j)}}\sum_k C(x-\xi_k, n_j)\cos(2\pi n_j t + \phi_{kj})\right], \tag{2}$$

where $C(\xi, n) = e^{-2Kn|\xi|/U} = COH_D^2(\xi, n)$, $COH_D(\xi, n) = e^{-Kn|\xi|/U}$. K is the coherence decaying coefficient, $S(n)$ is the target spectrum, ξ_k is the generation spot, ξ is the distance between two generated spots, n_j is the frequency, ϕ_{kj} is the starting phase which is uniformly distributed between 0 and 2π. Kovacs *et al.* [9] also suggested that the decaying coefficient can be taken as 4·5 for longitudinal and 7·5 for transverse velocity components. The buffeting loads along the bridge deck can be calculated by substituting the generated fluctuation wind velocities into equation (1).

2.2. SELF-EXCITED LOADS

The self-excited loads are caused by interaction between the wind motion and the structure. It involves the interaction of aerodynamic and inertial forces with the elastic structure such that the aerodynamic forces inject additional energy into the oscillating structure and increase the magnitude of vibration sometimes to catastrophic levels. It has been a tradition that the self-excited loads are expressed in the form of indicial functions as suggested by Scanlan [10]. However, Lin [11] considers that there are some redundancies in the classical formulations. Based on the assumptions that the self-excited loads are generated by linear mechanism, Lin suggests another simple mathematical model for self-excited forces for investigation of the aerodynamic stability of long-span suspension bridges. The self-excited loads are expressed in terms of convolution integrals between bridge deck motion and impulse response function which is shown to be equivalent to classical indicial function type representation. Lin's model can be summarized as

$$M_{se}(t) = M_\alpha(t) + M_h(t) = \int_{-\infty}^{t} f_{Mh}(t-\tau)h(\tau)\,d\tau + \int_{\infty}^{t} f_{M\alpha}(t-\tau)\alpha(\tau)\,d\tau, \tag{3a}$$

$$L_{se}(t) = L_\alpha(t) + L_h(t) = \int_{-\infty}^{t} f_{Lh}(t-\tau)h(\tau)\,d\tau + \int_{\infty}^{t} f_{L\alpha}(t-\tau)\alpha(\tau)\,d\tau, \tag{3b}$$

$$D_{se}(t) = D_\alpha(t) + D_p(t) = \int_{-\infty}^{t} f_{Dp}(t-\tau)p(\tau)\,d\tau + \int_{\infty}^{t} f_{D\alpha}(t-\tau)\alpha(\tau)\,d\tau, \tag{3c}$$

where $f_{M\alpha}(t), f_{Mh}(t), f_{L\alpha}(t), f_{Lh}(t), f_{D\alpha}(t)$, and $f_{Dp}(t)$ are response functions due to unit impulse displacement α, h and p. From these equations, it is seen that the aerodynamic coupling of the modes is induced by $M_h(t)$, $L_\alpha(t)$ and $D_\alpha(t)$.

Applying the Fourier transform to equations (3) and then comparing it with Scanlan's notion in terms of aerodynamic derivatives, the relationship between transfer functions and aerodynamic derivatives can be obtained as

$$F_{M\alpha}(\omega) = \rho B^4 \omega^2 [A_3^* + i A_2^*], \qquad F_{Mh}(\omega) = \rho B^3 \omega^2 [A_4^* + i A_1^*], \tag{4a, b}$$

$$F_{L\alpha}(\omega) = \rho B^3 \omega^2 [H_3^* + i H_2^*], \qquad F_{Lh}(\omega) = \rho B^2 \omega^2 [H_4^* + i H_2^*], \tag{4c, d}$$

$$F_{D\alpha}(\omega) = \rho B^3 \omega^2 [P_3^* + i P_2^*], \qquad F_{Dp}(\omega) = \rho B^2 \omega^2 [P_3^* + i P_2^*]. \tag{4e, f}$$

Here A_i^*, H_i^* and P_i^* $(i = 1, 4)$ are non-dimensional flutter derivatives obtained by wind tunnel tests on a cross-section of the deck.

From classical airfoil theory, the transfer functions may be reasonably approximated by rational functions, specifically for transfer functions of first order linear filters. The transfer functions $F_{M\alpha}$ can, therefore, be expressed as

$$F_{M\alpha}(v) = \rho B^2 U^2 \left[C_1 + \mathrm{i}\,\frac{2\pi C_2}{v} + \sum_{k=3}^{n} C_k \frac{4\pi^2 + \mathrm{i}2\pi d_k v}{d_k^2 v^2 + 4\pi^2} \right]. \tag{5}$$

Comparing equation (5 with equation (4), the flutter derivatives can be obtained as

$$A_3^* = v^2 \left(\frac{C_1}{4\pi^2} + \sum_{k=3}^{n} \frac{C_k}{d_k^2 v^2 + 4\pi^2} \right), \qquad A_2^* = \frac{v}{2\pi} \left(C_2 + \sum_{k=3}^{n} \frac{C_k d_k v^2}{d_k^2 v^2 + 4\pi^2} \right), \tag{6, 7}$$

In the above equations, v is the reduced velocity and is defined as $v = 2\pi U/\mathrm{Bn}$ [11]. The unknown parameters C_k and d_k can be obtained from least-squares fitting of equations (6) and (7). In this paper, a total of six unknown parameters $C_i (i = 1, 6)$ are used to compose the first order linear filters. By taking the inverse Fourier transformation of the transfer functions, the time domain expression of impulse response functions can be obtained. Substituting these impulse response functions into equation (3) yields

$$M_\alpha(t) = \rho B^2 U^2 \left\{ C_1 \alpha(t) + C_2 \frac{B}{U} \alpha(t) + C_3 \int_{-\infty}^{t} \exp\left[-\frac{C_5 U}{B} (t - \tau) \right] \alpha(\tau)\, \mathrm{d}\tau \right.$$

$$\left. + C_4 \int_{-\infty}^{t} \exp\left[-\frac{C_6 U}{B} (t - \tau) \right] \alpha(\tau)\, \mathrm{d}\tau \right\}. \tag{8}$$

The other five items including $M_h(t)$, $L_\alpha(t)$, $L_h(t)$, $D_\alpha(t)$ and $D_p(t)$ can be obtained similarly. It should be noted that every set of parameters $C_i (i = 1, 6)$ for $M_\alpha(t)$, $M_h(t)$, $L_\alpha(t)$, $L_h(t)$, $D_\alpha(t)$, $D_p(t)$ is different.

2.3. REFINED MODEL OF WIND LOADS

In usual buffeting analysis, the oncoming wind flow is assumed to occur from the direction normal to the bridge span, i.e., the effective attack angle of wind is zero. However, during the buffeting process, the bridge deck has not only translational displacements but also rotations, which lead to the instantaneous changes of the attack angle between the bridge deck and the wind direction. The change in attack angle causes a change in wind loads on the bridge decks. For certain shapes of cross-sections of bridge decks, due to their sensitivity to wind direction, the effect of changes can be quite significant. Therefore, it is necessary to consider the effect of the changes in attack angle of the wind on the buffeting response of bridges.

In the buffeting analysis, the bridge deck is subjected to the mean part and fluctuating part of wind flow. At the same time, the point of attack of the generated wind loads, which are generally assumed as concentrated loads, is not necessarily at the centerline of the bridge deck but is related to wind frequency [12]. In this paper, the point of attack of wind loads is assumed to be at the $\frac{1}{4}$ chord point of the deck. The relationship between bridge deck motion and wind motion at time t is shown in Figure 2. From this figure, it can be seen that the effective attack angle α_e is

$$\alpha_e = \Psi - \alpha, \tag{9}$$

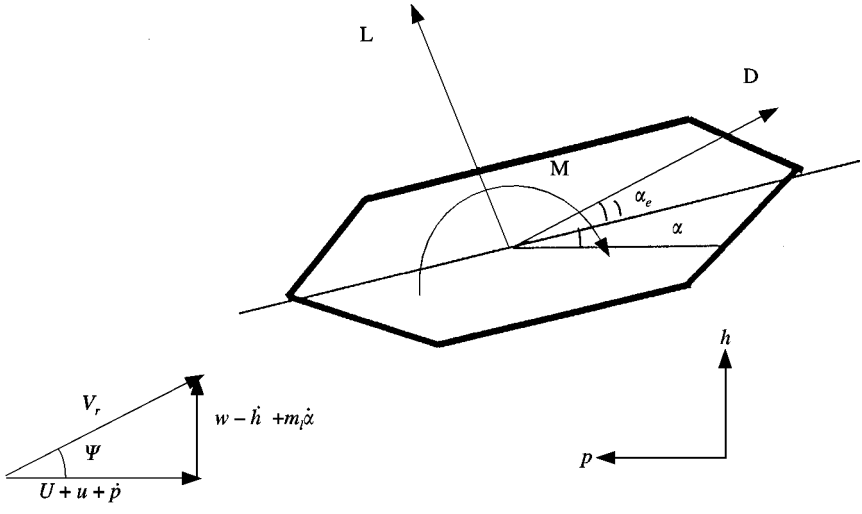

Figure. 2. The relationship between relative velocity V_r and effective attack angle α_e.

where

$$\tan \Psi = \frac{w - \dot{h} + m_l\dot{\alpha}}{U + u + \dot{p}}, \tag{10}$$

$$V_r(t) = \sqrt{(U + u + \dot{p})^2 + (w - \dot{h} + m_l\dot{\alpha})^2} = \text{relative velocity}. \tag{11}$$

$\dot{p}$, $\dot{h}$ and $\dot{\alpha}$ are the velocities of the bridge deck at time t with respect to the transverse, vertical and rotational directions, respectively; m_l the distance between point of attack of wind loads and centerline of bridge deck is taken as B/4 in this analysis; and α is the rotation angle of the bridge deck at time t. Considering the change in wind loads due to the instantaneous change in effective attack angle, the wind loads including lift, drag and moment at time t can be rewritten as

$$F_L(t) = L(t)\cos \Psi + D(t)\sin \Psi, \tag{12a}$$

$$F_D(t) = L(t)\sin \Psi - D(t)\cos \Psi, \tag{12b}$$

$$F_M(t) = M(t) \tag{12c}$$

It should be emphasized that the total lift, drag and moment is closely related to the effective attack angle of wind on the bridge deck because the lift, drag and moment coefficients as well as the aerodynamic derivatives of bridge deck vary with the wind attack angle. At every time step, the wind loads should be calculated based on the effective attack angle and corresponding wind tunnel test data.

3. STRUCTURAL IDEALIZATION

Normally, torsional stiffness of suspension bridges with box girder cross-sections is large, and hence the decks can be idealized as three-dimensional spine beam structures as shown

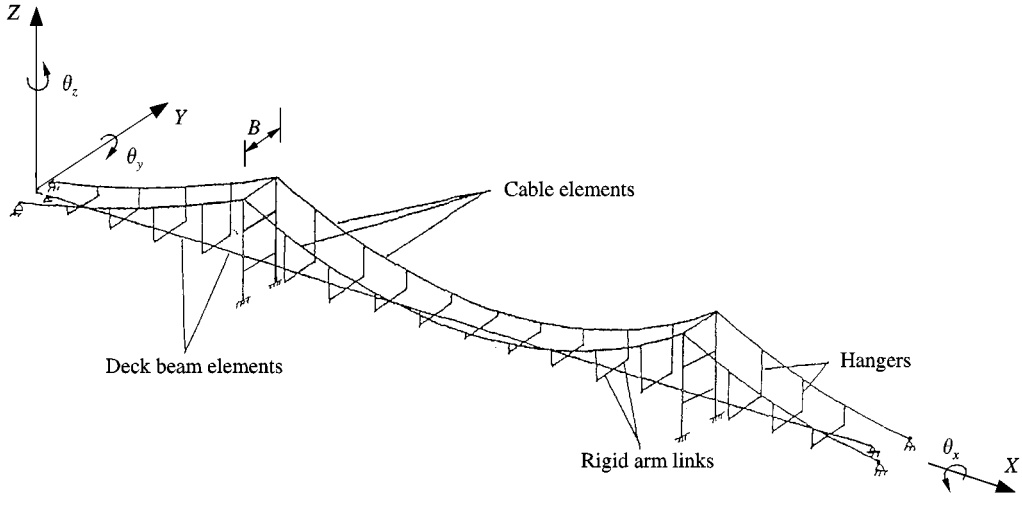

Figure. 3. Suspension bridge idealization in a three-dimensional space.

in Figure 3. The major structural elements of a suspension bridge are:

(a) *Cable element*: The length of cable spanning between hangers which is capable of resisting axial tensile force only.
(b) *Hanger element*: The vertical member between a cable node and the deck which is capable of resisting tensile force only.
(c) *Beam element*: The length of the deck spanning along the centerline of the bridge between a pair of nodes on the centerline. The hanger and deck elements are connected by horizontal rigid arms. They have bending stiffness in the vertical and lateral directions and are capable of resisting torsional stresses.
(d) *Tower element*: Each tower is represented by a three-dimensional framework fully fixed against movement at its base. In this frame, every element is a beam element having both bending stiffness and torsion stiffness.

Usually, bridge elements from the towers, deck, cables and hangers can be represented by two types of finite elements, i.e., spatial beam elements for towers and deck and cable elements for cables and hangers. In spite of the fact that the behavior of the material of the structural elements in a long-span bridge is linear elastic, the overall load–displacement relationship for the structure is non-linear [13]. This overall non-linear behavior originates from (i) the influence of cable sag to its equivalent modulus of elasticity, (ii) the effect of initial stresses on structural stiffness and (iii) the effect of large displacements on structural stiffness and loads.

3.1. CABLE ELEMENTS

Due to the very small bending stiffness, cable elements can be regarded as elements capable of resisting axial force only without any bending moment. In three-dimensional analysis, cable elements are composed of two nodes that have a total of six degrees of freedom as shown in Figure 4. For a cable element, the displacement vector $\{X\}$ can be written as $\{X\} = [u_i, v_i, w_i, u_j, v_j, w_j]^{\mathrm{T}}$.

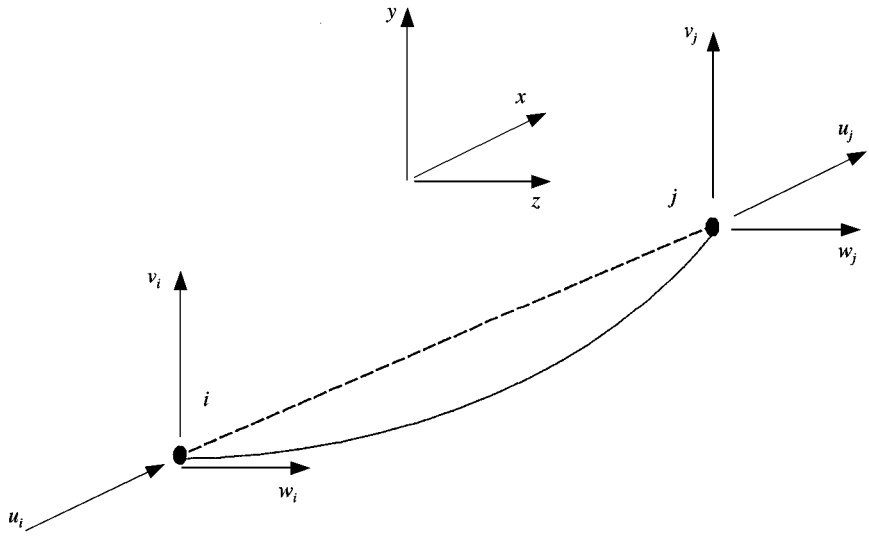

Figure. 4. Cable element at local co-ordinate system.

The non-linear behavior of cable elements results from its sag phenomenon. The axial stiffness of cable elements is affected by the cable sag that is greatly influenced by the amount of tension in the cable. When the cable tension increases, the sag decreases and apparent axial stiffness increases. In this paper, an equivalent straight chord member with an equivalent modulus of elasticity that combines both the effects of material and geometric deformations is used to account for this variation in cable axial stiffness [14]. The equivalent cable modulus of elasticity is given by

$$E_{eq} = \frac{E}{1 + ((\rho g l)^2 / 12\sigma^3)E} \tag{13}$$

in which E_{eq} is the equivalent modulus, E is the Young's modulus of cable material, ρ is the density of the cable, l is the horizontal projected length and σ is the tension stress of the cable. The total stiffness matrix of a cable element is, therefore, a combination of standard geometric stiffness matrix and elastic stiffness matrix.

3.2. BEAM ELEMENTS

When assuming small deformations in any structural system, the axial force and flexural stiffnesses of members in bending are usually considered to be uncoupled. However, when deformations are no longer small, there is an interaction between axial and flexural deformations in such members under the combined effect of axial force and bending moment. As a result, the effective stiffness of the member decreases for a compressive axial force and increases for a tensile force. In a similar manner, the presence of bending moments will also affect the axial stiffness of the member. In traditional linear analysis, this interaction or coupling effect is negligible. However, for flexural structures such as long-span suspension bridges, large displacements will occur. This interaction can be significant and should be considered in any non-linear analysis.

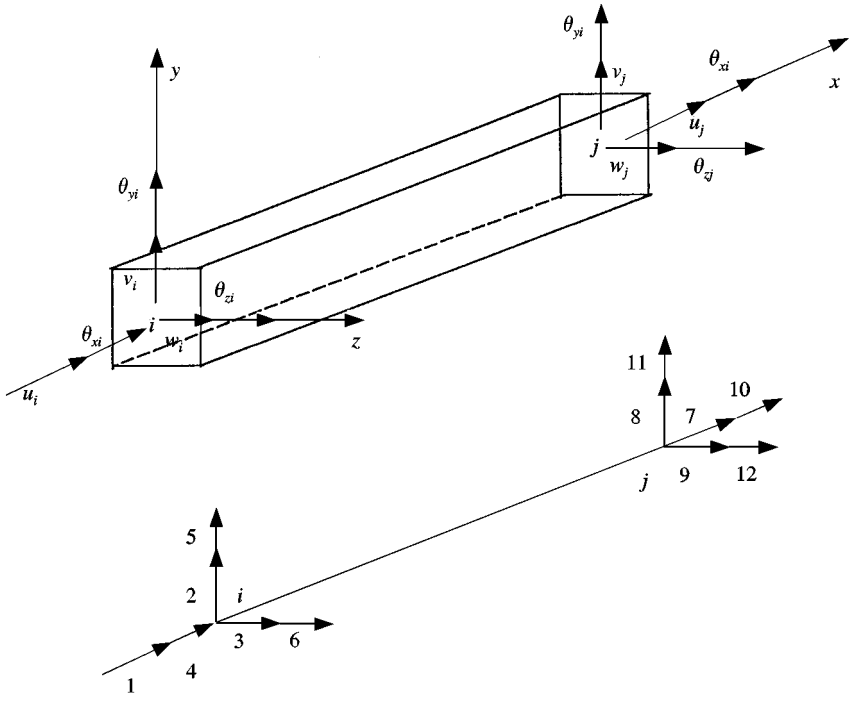

Figure. 5. Beam element at local co-ordinate system.

In three-dimensional analysis, a spatial beam element has 12 degrees of freedom as shown in Figure 5. For beam elements, the displacement vector $\{X\}$ can be written as

$$\{X\} = [u_i, v_i, w_i, \theta_{xi}, \theta_{yi}, \theta_{zi}, u_j, v_j, w_j, \theta_{xj}, \theta_{yj}, \theta_{zj}]^{\mathrm{T}}.$$

Analogous to that of cable elements, the stiffness of beam elements is composed of two parts: elastic stiffness and geometric stiffness. Based on large displacement theory, a geometric stiffness matrix of beam elements incorporating the contribution of axial force and bending moments has been derived by Pan *et al.* [15] and used in this analysis.

4. EQUATIONS OF MOTION

The equations of motion in terms of a nodal displacement vector $[U]$ for a bridge structural system under wind loads can be expressed in conventional matrix notation as

$$[M][\ddot{U}] + [C][\dot{U}] + [K][U] = [P], \tag{14}$$

where $[M]$ is a diagonal matrix containing the mass and mass moment inertia of all elements lumped at the nodes, $[C]$ the structural damping matrix taken as Rayleigh's damping, $[K]$ the structural stiffness matrix including elastic stiffness matrix and geometrical stiffness matrix, and $[P]$ the total wind load which includes buffeting wind loads $[P_{bu}]$ and self-excited wind loads $[P_{se}]$.

When equation (8) is observed more closely, it is found that the self-excited loads can be expressed in three parts: aerodynamic stiffness part, aerodynamic damping part and motion

history part, as follows:

$$M_\alpha(t) = P_{M\alpha,S}\alpha(t) + P_{M\alpha,D}\alpha(t) + P_{M\alpha}, \tag{15}$$

where

$$P_{M\alpha,S} = \rho B^2 U^2 C_1, \qquad P_{M\alpha,D} = \rho B^2 U^2 \frac{C_2 B}{U} = \rho B^3 U C_2, \tag{16a, b}$$

$$P_{M\alpha} = \rho B^2 U^2 \left\{ C_3 \int_{-\infty}^{t} \exp\left[-\frac{C_5 U}{B}(t-\tau) \right] \alpha(\tau)\,\mathrm{d}\tau \right.$$

$$\left. + C_4 \int_{-\infty}^{t} \exp\left[-\frac{C_6 U}{B}(t-\tau) \right] \alpha(\tau)\,\mathrm{d}\tau. \right. \tag{16c}$$

The other five load items in equation (3) can also be described analogously. Combining all the aerodynamic stiffness parts and damping parts together, the aerodynamic stiffness and damping matrix in the local co-ordinate system can be set-up. The aerodynamic stiffness matrix of an element can be written as

$$\frac{L}{2}\begin{bmatrix}
0 & 0 & 0 & 0 & 0 & 0 & 0 & 0 & 0 & 0 & 0 & 0 \\
0 & B_{Lh,S} & 0 & -B_{L\alpha,S} & 0 & 0 & 0 & 0 & 0 & 0 & 0 & 0 \\
0 & 0 & B_{Dp,S} & B_{D\alpha,S} & 0 & 0 & 0 & 0 & 0 & 0 & 0 & 0 \\
0 & -B_{Mh,S} & 0 & B_{M\alpha,S} & 0 & 0 & 0 & 0 & 0 & 0 & 0 & 0 \\
0 & 0 & 0 & 0 & 0 & 0 & 0 & 0 & 0 & 0 & 0 & 0 \\
0 & 0 & 0 & 0 & 0 & 0 & 0 & 0 & 0 & 0 & 0 & 0 \\
0 & 0 & 0 & 0 & 0 & 0 & 0 & 0 & 0 & 0 & 0 & 0 \\
0 & 0 & 0 & 0 & 0 & 0 & 0 & B_{Lh,S} & 0 & -B_{L\alpha,S} & 0 & 0 \\
0 & 0 & 0 & 0 & 0 & 0 & 0 & 0 & B_{Dp,S} & B_{D\alpha,S} & 0 & 0 \\
0 & 0 & 0 & 0 & 0 & 0 & 0 & -B_{Mh,S} & 0 & B_{M\alpha,S} & 0 & 0 \\
0 & 0 & 0 & 0 & 0 & 0 & 0 & 0 & 0 & 0 & 0 & 0 \\
0 & 0 & 0 & 0 & 0 & 0 & 0 & 0 & 0 & 0 & 0 & 0
\end{bmatrix}$$

and the aerodynamic damping matrix

$$\frac{L}{2}\begin{bmatrix}
0 & 0 & 0 & 0 & 0 & 0 & 0 & 0 & 0 & 0 & 0 & 0 \\
0 & B_{Lh,D} & 0 & -B_{L\alpha,D} & 0 & 0 & 0 & 0 & 0 & 0 & 0 & 0 \\
0 & 0 & B_{Dp,D} & B_{D\alpha,D} & 0 & 0 & 0 & 0 & 0 & 0 & 0 & 0 \\
0 & -B_{Mh,D} & 0 & B_{M\alpha,D} & 0 & 0 & 0 & 0 & 0 & 0 & 0 & 0 \\
0 & 0 & 0 & 0 & 0 & 0 & 0 & 0 & 0 & 0 & 0 & 0 \\
0 & 0 & 0 & 0 & 0 & 0 & 0 & 0 & 0 & 0 & 0 & 0 \\
0 & 0 & 0 & 0 & 0 & 0 & 0 & 0 & 0 & 0 & 0 & 0 \\
0 & 0 & 0 & 0 & 0 & 0 & 0 & B_{Lh,D} & 0 & -B_{L\alpha,D} & 0 & 0 \\
0 & 0 & 0 & 0 & 0 & 0 & 0 & 0 & B_{Dp,D} & B_{D\alpha,D} & 0 & 0 \\
0 & 0 & 0 & 0 & 0 & 0 & 0 & -B_{Mh,D} & 0 & B_{M\alpha,D} & 0 & 0 \\
0 & 0 & 0 & 0 & 0 & 0 & 0 & 0 & 0 & 0 & 0 & 0 \\
0 & 0 & 0 & 0 & 0 & 0 & 0 & 0 & 0 & 0 & 0 & 0
\end{bmatrix}$$

Regarding the motion history parts, it can be seen that the items involve convolution integrals of velocities. These series integrals can be summarized as

$$I_j = \int_{-\infty}^{t_j} \exp[(-c_i U/B)(t_j - \tau)]\dot{\delta}(\tau)\,\mathrm{d}\tau. \tag{17}$$

It can be seen that for calculating their values, the integral I_j must be evaluated at every time step t_j which is quite time consuming. Besides, the motion history for all elements must be stored, thus occupying a large memory of the computer. To tackle these difficulties, a recursive algorithm for evaluating the integral is derived as follows:

$$I_j = \exp[(-c_i U/B)(t_j - t_{j-1})]I_{j-1} + \exp[(-c_i U/2B)(t_j - t_{j-1})]\Delta\delta_{j-1}. \tag{18}$$

From the above equation, it can be seen that only the quantities involving I_{j-1} and δ_{j-1} at time t_{j-1} need to be stored for evaluating I_j.

In summary, the motion equation can be rewritten as

$$[M][\ddot{U}] + \{[C] - [C_{se}]\}[\dot{U}] + \{[K_e] + [K_g] - [K_{se}]\}[U] = [P_{bu}] + [P_{seh}], \tag{19}$$

where $[K_e]$ is the elastic stiffness matrix, $[K_g]$ the geometrical stiffness matrix, $[P_{bu}]$ the buffeting load vector, $[K_{se}]$ the aerodynamic stiffness matrix due to self-excited wind loads, $[C_{se}]$ the aerodynamic damping matrix due to self-excited wind loads, and $[P_{seh}]$ the self-excited wind loads related to motion history.

5. CASE STUDY—BUFFERING ANALYSIS OF TSING MA BRIDGE

The Tsing Ma Bridge (Figure 6) [16], an integral component of the Airport Core Projects in Hong Kong, was opened to traffic in 1997. This bridge has an overall length of 2200 m with a main suspended span of 1377 m. It is the longest suspension bridge carrying both road and rail traffic in the world. The main support towers are concrete structures over 200 m high. The two main cables, each of which was formed from nearly 40,000 individual

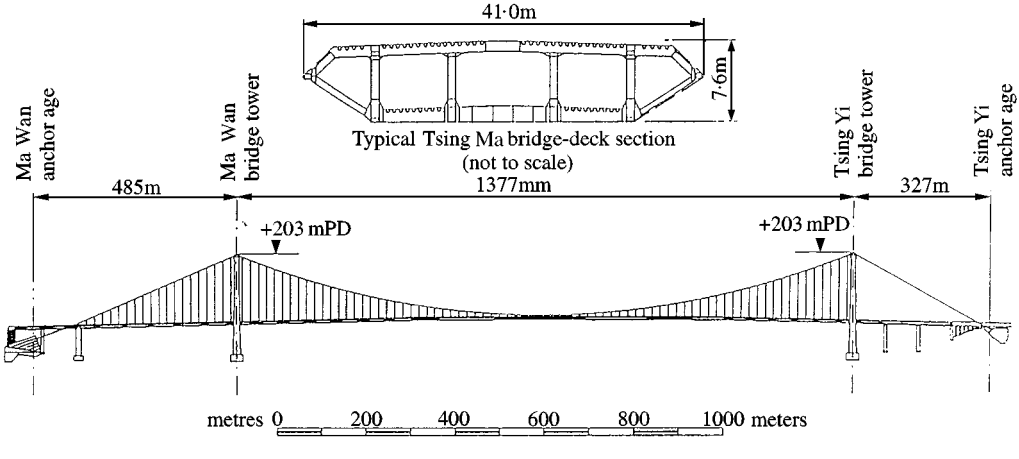

Figure. 6. General layout of the Tsing Ma Bridge (extracted from reference [16]).

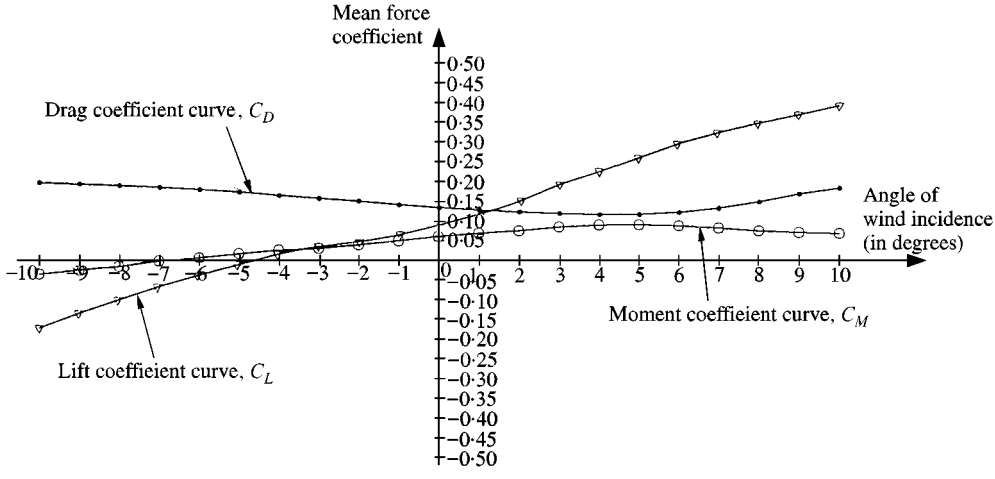

Figure. 7. Drag, lift and moment coefficient curves of the Tsing Ma Bridge.

TABLE 1

Aerodynamic coefficients

	C_1	C_2	C_3	C_4	C_5	C_6
M	0·26412	− 0·51993	0·16645	0·29121	13·43210	5·87260
I	− 1·08827	− 2·79466	0·99064	1·06341	13·09312	229·358

steel wires of 5 mm diameter, are approximately 1 m in diameter. The typical steel box-girder deck is 41 m in width, carrying a dual three-lane expressway together with double rail tracks for the Airport Railway.

The drag, lift and moment coefficient of the typical deck of the Tsing Ma Bridge are shown in Figure 7. Based on the wind tunnel test data [16], the unknown aerodynamic coefficients C_1–C_6 have been determined and tabulated in Table 1.

In the following study, Simiu spectrum and Panofsky–McCormick spectrum with a mean wind speed of $U = 60$ m/s are chosen as the along-wind and vertical target spectrum of wind fluctuations respectively. The Newmark-β step-by-step numerical integration algorithm with $\gamma = 0{\cdot}5$ and $\beta = 0{\cdot}25$ is used to calculate the buffeting responses of the Tsing Ma Bridge. The number of total time steps is taken as 1000 with a time interval of 0·2 s.

The buffeting responses of the Tsing Ma Bridge are calculated in two cases: (i) without consideration of effective attack angle of the wind and (ii) with consideration of effective attack angle of the wind. The corresponding responses at the mid-span and quarter-span under a mean wind velocity of $U = 60$ m/s are shown in Figures 8–15.

From these figures, it can be seen that whether it is in case (i) or (ii), the peak vertical displacement at quarter span is much larger than at mid-span while the peak torsional response is much smaller. This phenomenon is probably due to the fact that the first vibration mode excited makes the greatest contribution to structural response. For the Tsing Ma Bridge, the first vertical vibration mode shape is antisymmetrical while the first rotational vibration mode shape is symmetrical. The peak vertical responses, therefore, occur at quarter-span rather than mid-span while the peak rotational responses occur at mid-span.

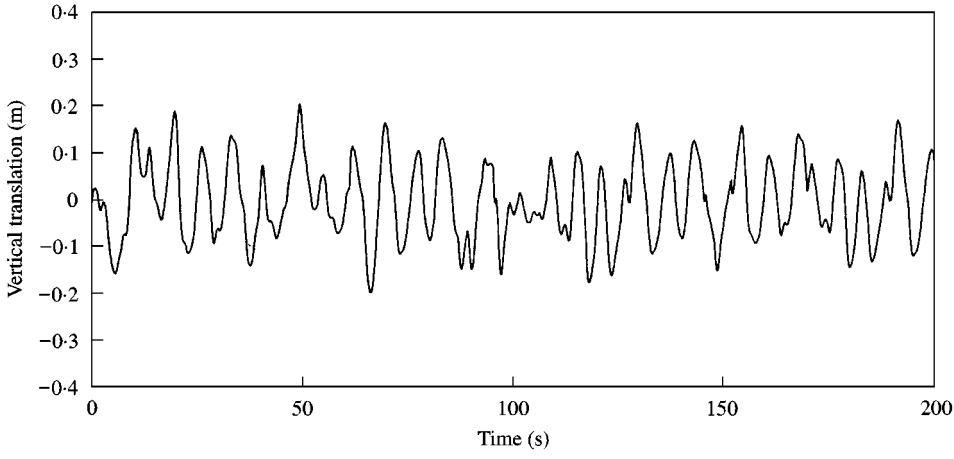

Figure. 8. Vertical response at mid-span without consideration of attack angle.

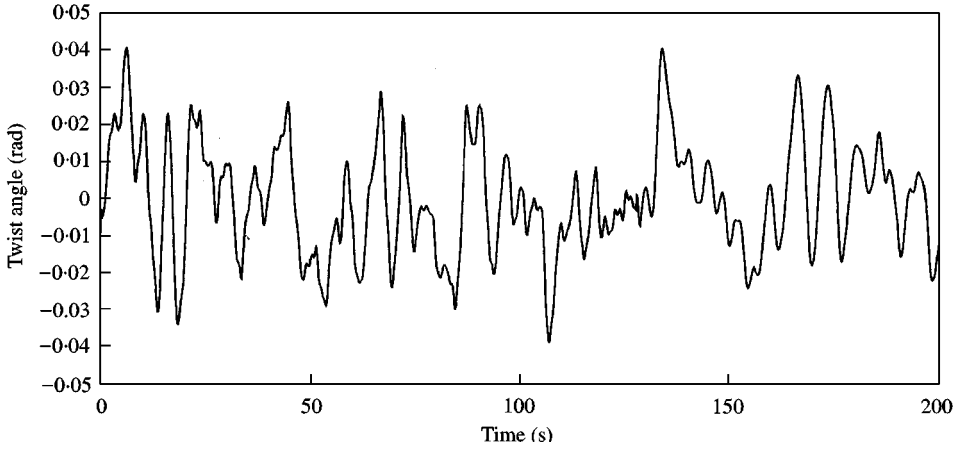

Figure. 9. Torsional response at mid-span without consideration of attack angle.

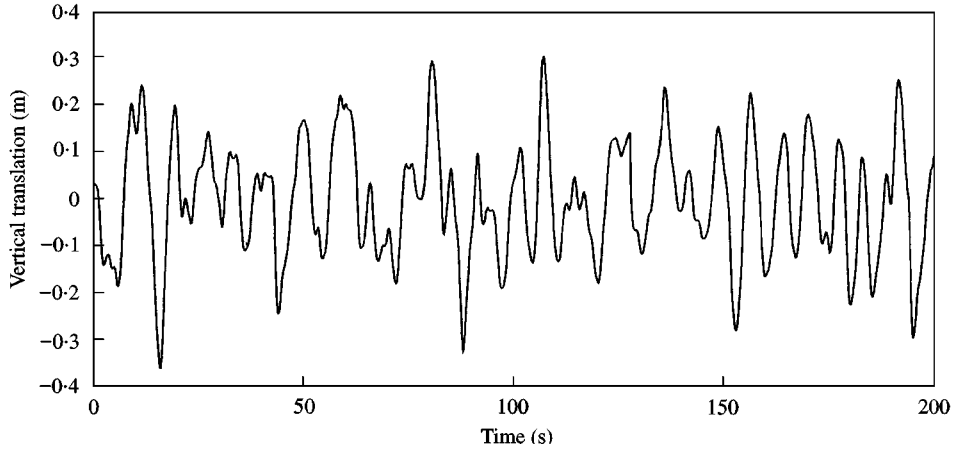

Figure. 10. Vertical response at quarter-span without consideration of attack angle.

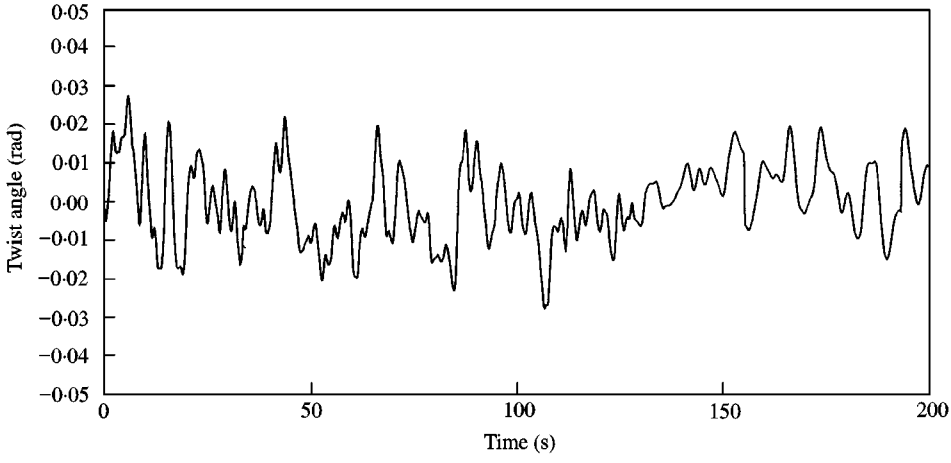

Figure. 11. Torsional response at quarter-span without consideration of attack angle.

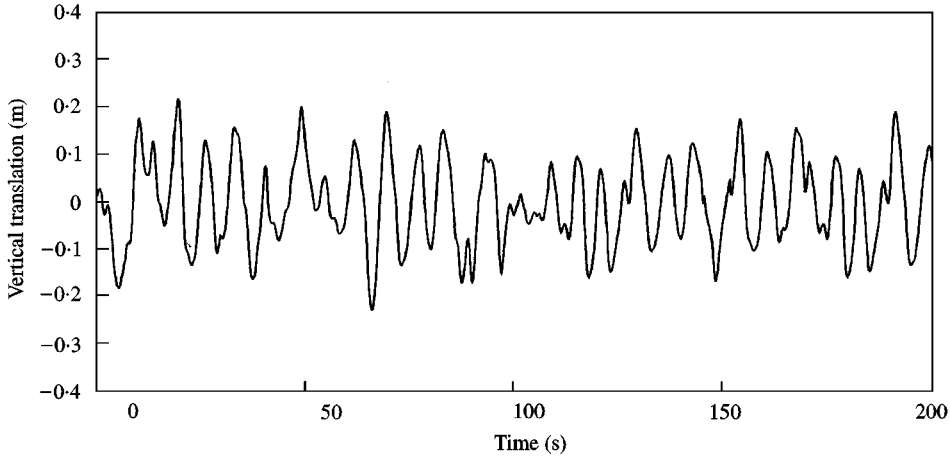

Figure. 12. Vertical response at mid-span with consideration of attack angle.

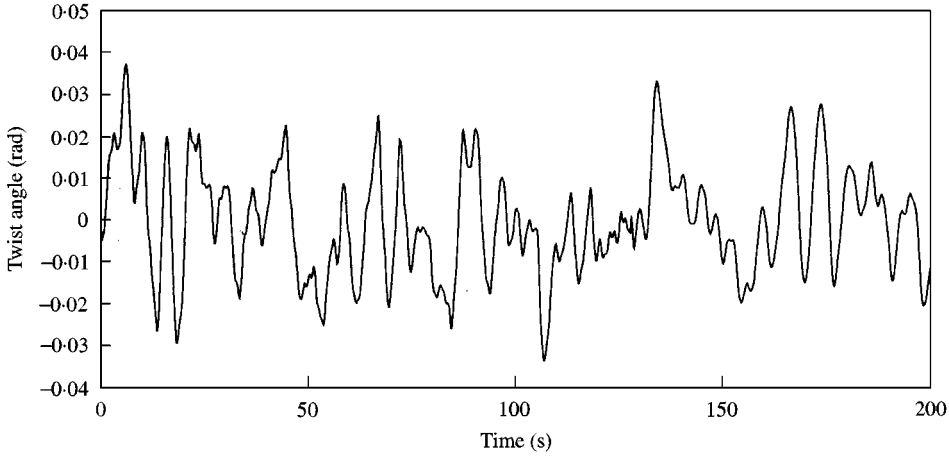

Figure. 13. Torsional response at mid-span with consideration of attack angle.

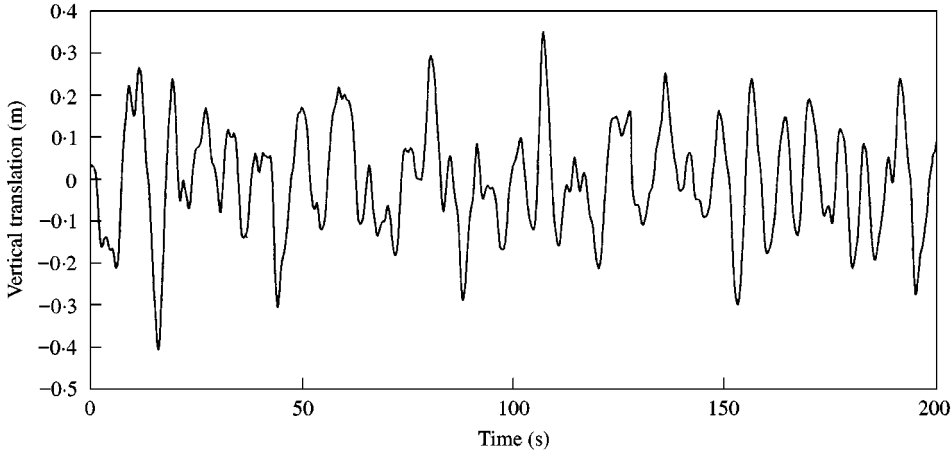

Figure. 14. Vertical response at quarter-span with consideration of attack angle.

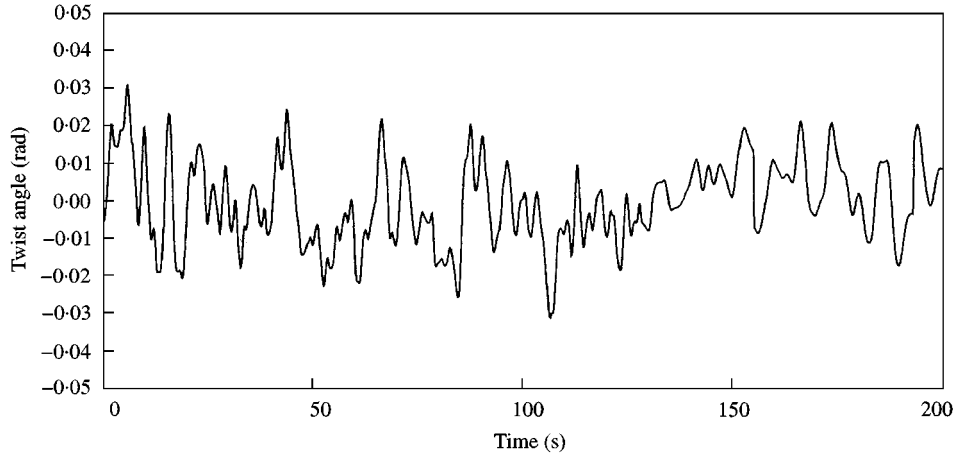

Figure. 15. Torsional response at quarter-span with consideration of attack angle.

It can also be seen that considering the effect of wind attack angle apparently leads to larger buffeting responses. For mid-span, the peak vertical and torsional buffeting responses increase by 11·7 and 9·9% and for quarter-span, the increases are 11·9 and 10·8% respectively. On the other hand, when the effect of wind attack angle is considered, the root-mean-square value of the vertical responses at mid-span and quarter-span are 0·091 and 0·131 m respectively. Compared to the values calculated without considering wind attack angle, which are alternatively 0·085 and 0·127 m, the differences are only 5·8 and 3·1%. From these results, it is found that for the Tsing Ma Bridge, the instantaneous change in wind attack angle leads to greater increase in the peak vertical and rotational response but it has less effect on the whole buffeting process.

According to classic buffeting theory, the root-mean-square values of vertical responses at mid-span and quarter-span are respectively 0·094 and 0·133 m. Through comparison, it can be seen that whether the instantaneous change in wind attack angle is considerated or not, the calculated root-mean-square values of buffeting response are in good agreement

with the results obtained by traditional buffeting theory, with a difference of not more than 10%. Furthermore, when compared with results computed without considering wind attack angle, the results taking into account the instantaneous change in wind attack angle are closer to those obtained using the classic buffeting theory.

It should be emphasized that the effect of effective attack angle of wind on the buffeting responses for the Tsing Ma Bridge may not be extended to other cases, as it depends very much on the shape of the cross-section of the bridge deck. For other bridge decks, the lift, drag and moment coefficients as well as the aerodynamic derivatives may be quite different from those of the Tsing Ma Bridge. Hence, the effect of instantaneous change in wind attack angle on the buffeting responses may be quite different.

6. CONCLUDING REMARKS

In this paper, a time domain buffeting method is presented to analyze the buffeting response of long-span suspension bridges under turbulent wind. In the bridge model, all geometrical non-linearities such as cable sag, axial force–bending moment interaction in the bridge deck and towers as well as changes in the bridge geometry due to large displacements are considered. Based on Scanlan's method, the wind loads including buffeting loads and self-excited loads are described as functions of aerodynamic parameters obtained through wind tunnel tests and converted into the time domain by using a computer simulation technique. The computational results are, therefore, more accurate than those obtained by the classic spectrum method which is limited in linearization scope. In addition, this method can also reveal the response process of the entire bridge which may be useful in other studies such as the structural health monitoring system and the real-time traffic control system. Compared with the results obtained by classic buffeting theory through an example bridge, the Tsing Ma Bridge, the validity of the proposed method is verified.

In order to investigate the effect of an instantaneous change in effective attack angle of turbulent wind on bridge buffeting response, a more refined model of wind loads has been established. It is found that for the Tsing Ma Bridge, as instantaneous change in attack angle of the wind leads to larger peak buffeting responses but has a lesser effect on the entire buffeting process.

REFERENCES

1. A. G. DAVENPORT 1962 *Journal of the structural Division*, ASCE **88**, 233–268. Buffeting of a suspension bridge by stormy winds.
2. J.-G. BELIVEAU, R. VAICAITIS and M. SHINOZUKA 1977 *Journal of the Structural Division*, ASCE **103**, 1189–1205. Motion of suspension bridge subject to wind loads.
3. R. H. SCANLAN and J. J. TOMKO 1971 *Journal of the Structural Division*, ASCE **97**, 1717–1737. Airfoil and bridge flutter derivatives.
4. R. H. SCANLAN and R. H. GADE 1977 *Journal of the Structural Division*, ASCE **103**, 1867–1883. Motion of suspended bridge spans under gust wind.
5. R. H. SCANLAN 1983 *Journal of Structural Engineering*, ASCE **109**, 2829–2837. Aeroelastic simulation of bridges.
6. Y. K. LIN and J. N. YANG 1983 *Journal of Structural Mechanics*, ASCE **8**, 1–15. Stability of bridge motion in turbulent winds.
7. Y. K. LIN and J. N. YANG 1983 *Journal of Engineering Mechanics*, ASCE **109**, 586–603. Multimode bridge response to wind excitations.
8. T. J. A. AGAR 1988 *Computer & Structures* **30**, 593–600. The analysis of aerodynamic flutter of suspension bridges.
9. I. KOVACS, H. S. SVENESSON and E. JORDET 1992 *Journal of Structural Engineering*, ASCE **118**, 147–168. Analytical aerodynamic investigation of helgeland cable-stayed bridge.

10. R. H. SCANLAN, J. G. BELIVEAU and K. S. BUDLONG 1974 *Journal of Engineering Mechanics*, ASCE **100**, 657–672. Indicial aerodynamic functions for bridge decks.
11. C. G. BUCHER and Y. K. LIN 1988 *Journal of Engineering Mechanics*, ASCE **114**, 2055–2071. Stochastic stability of bridges considering coupled modes.
12. J. C. SANTOS 1993 *Proceedings of Third AsiaPacific Symposium on Wind Engineering*, *Hong Kong*, 211–216. Gust response of a long span bridge by the time domain approach.
13. J. F. FLEMING 1979 *Computers & Structures* **10**, 621–635. Nonlinear static analysis of cable stayed bridge structures.
14. H. J. ERNST 1965 *Der Bauingenieur* **40**, 52–55. Der E-Modul von Seilen under Beruecksichtigung des Durchhanges (in German).
15. J. Y. PAN and Q. G. CHENG 1994 *Journal of Civil Engineering*, ASCE **27**, 1–9. Finite displacement analysis of large suspension bridge.
16. C. K. LAU and K. Y. WONG 1997 *Proceeding of the Fourth International Kerensky Conference on Structures in the New Millennium*, *Hong Kong*, 131–138. Aerodynamic stability of Tsing Ma Bridge.